A Case of Strong Metal–Support Interactions: Combining Advanced Microscopy and Model Systems to Elucidate the Atomic Structure of Interfaces**

Marc G. Willinger, Wei Zhang, Oleksandr Bondarchuk, Shamil Shaikhutdinov,* Hans-Joachim Freund, and Robert Schlögl*

Abstract: *A symbiosis of advanced scanning probe and electron microscopy and a well-defined model system may provide a detailed picture of interfaces on nanostructured catalytic systems. This was demonstrated for Pt nanoparticles supported on iron oxide thin films which undergo encapsulation by supporting oxide as a result of strong metal–support interactions.*

One of the most successful approaches for tailoring the catalytic function of metal nanoparticles is to select a suitable support. There is a whole class of "non-innocent" supports that interact upon suitable synthesis with the metal particles by the so-called strong metal–support interaction (SMSI).[1] Some of the SMSI effects involve the formation of hetero-interfaces between the metal particle and a semiconducting (oxidic) thin layer moderating the electronic structure and thus changing the adsorptive properties of the system.[2] Decoration of metal particles by oxide usually suppresses catalytic activity, but, in certain cases, it results in an enhanced reactivity and unparalleled selectivity depending on how the gas phase sets the chemical potential.[3] Despite its well-known phenomenological effects, an atomic level understanding of the SMSI states is still missing. In particular, theory is not yet in position to predict its function.

With the advent of aberration-corrected transmission electron microscopy (TEM),[4] new opportunities have opened up for investigating heterogeneous catalysts at the atomic scale. In particular, the atomic resolution at surfaces has been revealed,[5] which was previously only available by scanning tunneling microscopy (STM) on planar systems.[6]

To provide an experimental basis for an atomistic understanding of the SMSI effects, we applied here advanced electron microscopies (STM and TEM) to a model system consisting of Pt nanoparticles on a well-ordered $Fe_3O_4(111)$ film. It has previously been shown by STM that, upon annealing in ultrahigh vacuum (UHV), the top facets of the Pt particles are covered with a layer which is virtually identical to a monolayer FeO(111) film on Pt(111)[6b,7] (Figure 1 A,B).

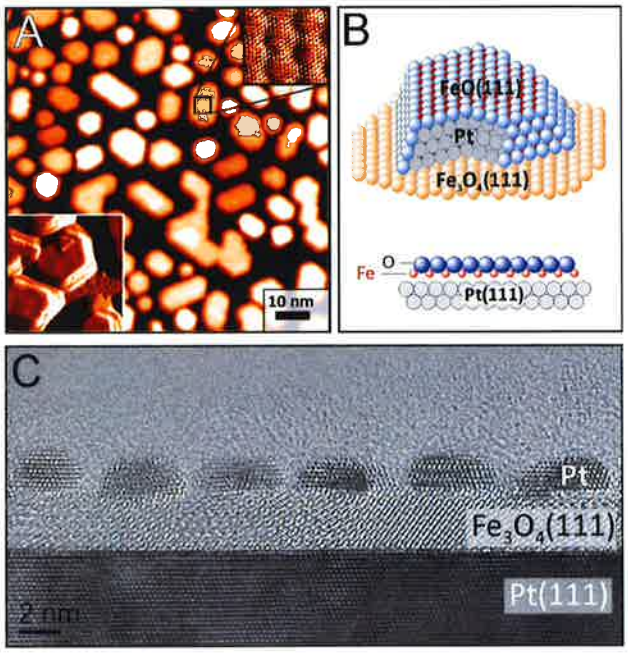

Figure 1. A) A typical STM image of a $Pt/Fe_3O_4(111)$ surface after annealing in vacuum at 850 K. B) Representation of an encapsulated Pt particle and a cross-view of an FeO(111) monolayer on Pt(111). C) High resolution TEM image of $Pt/Fe_3O_4(111)$ in cross-section.

Complementary reactivity studies at near atmospheric pressures showed a higher activity of the encapsulated Pt particles in CO oxidation compared to the clean Pt particles.[3d] Further studies[8] showed that a monolayer FeO(111) film grown on a Pt(111) single crystal is much more active than clean Pt(111) and several nm-thick $Fe_3O_4(111)$ films, thus indicating that the reactivity is intimately connected to the atomic structure of ultrathin iron oxide films formed on Pt. However, a confirmation of STM data by direct measurement of the elemental composition was so far not achieved. Furthermore, there are open questions regarding the interface structure between the Pt particles and the overgrowing film on one side and the $Fe_3O_4(111)$ support on the other. Finally, the mechanism of the encapsulation remains unclear.

[*] Dr. M. G. Willinger, Dr. W. Zhang, Dr. O. Bondarchuk, Dr. S. Shaikhutdinov, Prof. Dr. H.-J. Freund, Prof. Dr. R. Schlögl
Fritz Haber Institute of the Max Planck Society
Faradayweg 4–6, 14195 Berlin (Germany)
E-mail: willinger@fhi-berlin.mpg.de
shaikhutdinov@fhi-berlin.mpg.de

[**] This work has been supported by the Deutsche Forschungsgemeinschaft. The authors wish to recognize Dr. Yu. Martynova (FHI) and A. Yasuhara (JEOL Ltd) for technical assistance.

Figure 1C displays a typical high-resolution TEM (HRTEM) image of the $Pt/Fe_3O_4(111)$ system in cross-section, showing a good epitaxy between a Pt(111) substrate, an $Fe_3O_4(111)$ film, and Pt nanoparticles (Supporting Information, Figure S1). The particle morphology and size are very similar to those obtained by STM. To elucidate the atomic structure of interfaces, high-angle annular dark-field scanning TEM (HAADF STEM) images have been recorded (Figure 2).

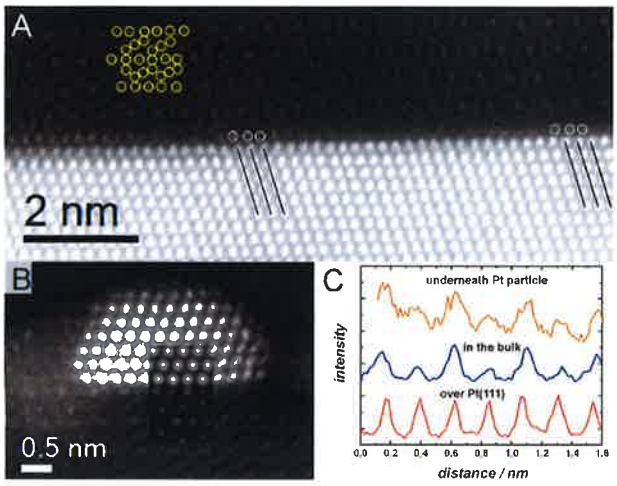

Figure 2. HAADF STEM images of interfaces between A) a Pt(111) substrate and an $Fe_3O_4(111)$ film (A) and B) an oxide film and a supported Pt particle. The Fe atomic columns in the $Fe_3O_4(111)$ bulk are marked by circles in (A). Registry variations of the interfacial oxide layer with respect to the Pt(111) surface are highlighted. C) Intensity profiles measured for the atomic columns in the first oxide layer over a Pt(111) substrate (red), and underneath the Pt particle shown in image B (orange). The intensity profile along the Kagomé layer in the bulk of the $Fe_3O_4(111)$ film is shown for comparison (blue).

We first address the interface between the Pt(111) support and the $Fe_3O_4(111)$ film. Figure 2A shows that the first layer of atomic columns just above the bright Pt columns shows considerably weaker contrast. Furthermore, this layer exhibits a larger lattice constant than of Pt(111), thus resulting in a registry variation with respect to the underlying layer and in associated contrast modulation induced by this lattice mismatch. Therefore, we assign this layer to the iron oxide phase. It is instructive here to recall that the bulk structure of $Fe_3O_4(111)$ (Supporting Information, Figure S2) may be viewed as closed-packed monolayers (ML) of oxygen ions with a 2.97 Å lattice constant separated by two different iron layers which alternate in stacking order.[9] One is a mixtrigonal layer that in turn consists of three Fe layers $^1/_4$ ML each ($^3/_4$ ML in total); and the second one is a so-called Kagomé layer ($^3/_4$ ML).

As a starting point to a structural analysis, we employed the model, previously proposed by Roddatis et al.[10] on the basis of high-resolution TEM images, in which the Kagomé layer is placed over Pt(111). However, the intensity of the Fe columns in a Kagomé layer has to alternate according to the density of the Fe atoms along the columns (in a 2:1 ratio; Supporting Information, Figure S2). This is clearly observed in the film bulk (see line profiles in Figure 2C), but it is definitely not the case for the interfacial layer. The adjacent columns exhibit near equal intensity, thus suggesting that the interfacial layer, in fact, consists of a close-packed Fe layer like in FeO(111). The interlayer distance measured between the Fe and Pt columns (2 Å on average) is too small for having any O-layer (hardly visible in TEM) in between. Bearing in mind that a FeO(111) monolayer on Pt(111) is stacked as O-Fe-Pt (Figure 1B), and this layer is first prepared on Pt(111) prior to a subsequent layer-by-layer growth of the $Fe_3O_4(111)$ film, we conclude that the film–substrate interface consists of a close-packed Fe-layer over Pt(111).

Applying the same approach to the interface between a Pt particle and a $Fe_3O_4(111)$ film, we found that it consists of a Kagomé layer exposed to the Pt(111) facet of the particle as shown in Figure 2B. Indeed, this interfacial layer exhibits the above-mentioned intensity oscillation (Figure 2C). Again, the interlayer distance between the Pt and Fe columns (ca. 2 Å) indicates the absence of an O-layer in between.

The difference between the two interfaces (Pt(111)/$Fe_3O_4(111)$ versus $Fe_3O_4(111)$/Pt(111)) may, in first approximation, be explained by the preparation: The film growth involved annealing in 10^{-6} mbar O_2 at about 1000 K, whereas the Pt particles were heated in UHV to 850 K only. More intriguing is the finding that a Pt particle sits on top of the Kagomé layer, which is not the most stable termination of a pristine $Fe_3O_4(111)$ film. It has previously been shown that the $Fe_3O_4(111)$ surface is represented by a $^1/_4$ ML Fe in a (2×2) structure over the O-layer (Supporting Information, Figure S1),[9] although some small ill-defined clusters may be present at the film surface.[11] Therefore, upon Pt deposition, particle growth and subsequent high-temperature annealing, the surface Fe and O layers are removed for the Pt(111) layer in the particle to bind the Kagomé layer, which is the next Fe-containing layer below the topmost Fe-layer in the pristine film. It therefore appears that the interface between Pt(111) and $Fe_3O_4(111)$ is formed in such a way that it maximizes the number of Pt/Fe bonds. Indeed, the amount of Fe in the Kagomé layer is three times higher than in the terminating Fe layer. The preferential formation of the Pt–Fe bonds at the interface may also be traced back from simplified metal–oxide junction considerations. The work function of Fe_3O_4-(111) (ca. 5.5 eV) is lower than of Pt(111) (5.93 eV), and therefore the contact between Pt and iron oxide would result in electron transfer from oxide to Pt, which will drive the positively charged Fe ions to be at the interface.[12]

We now address the surface structure of the supported Pt particles studied by HRTEM. Figure 3A clearly shows that the particle surface exhibits a low-contrast, uniform atomic layer with the periodicity of atomic columns obviously larger than that of underlying Pt(111). This finding is fully consistent with the STM results, suggesting the formation of an FeO-(111) layer having a larger lattice constant (ca. 3.05 Å) than Pt(111) (2.78 Å). Using the distance between the Pt columns in Pt(111) as an internal reference (2.4 Å), the measured distance between the columns in the surface overlayer (ca. 2.7 Å) agrees well with 2.62 Å expected for the Fe columns in the FeO(111) monolayer.

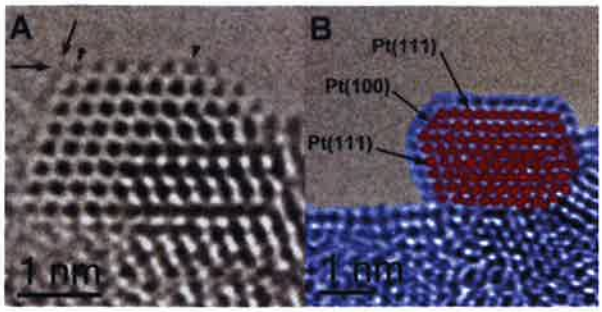

Figure 3. HRTEM images of Pt particles supported by $Fe_3O_4(111)$ in the SMSI state. A) The long arrows indicate the encapsulated layer, and the short arrows highlight the relative displacement of the topmost row of atoms with respect to the Pt atoms underneath. B) Colorized image to illustrate continuous encapsulation layer on different facets of a Pt particle as indicated. (The original images are shown in the Supporting Information, Figure S3).

Furthermore, the HRTEM images show that the side facets, which could not be resolved by STM, are covered essentially by the same oxide layer (Figure 3 B; Supporting Information, Figure S3). Although this has been proposed on the basis of CO adsorption experiments[7] and previous STM studies of FeO(111) films on a Pt(100) substrate,[13] the HRTEM images provide direct evidence for the encapsulation of the whole Pt particle by the FeO(111) layer.

The chemical composition of the surface layer was examined by electron energy loss spectroscopy (EELS) in the STEM mode having certain advantage over conventionally used energy-dispersive X-ray spectroscopy.[14] Figure 4 shows the EELS spectrum obtained from interior regions of the $Fe_3O_4(111)$ film, showing the K-edge of O and the L-edge of Fe approximately at 530 eV and 710 eV, respectively. Essentially the same features with a much lower intensity are observed in the EELS spectrum at the surface of the imaged Pt particle, thus suggesting that the encapsulated layer seen by HRTEM (Figure 3) and STM (Figure 1 A) contains both oxygen and iron, although its stoichiometry cannot be determined precisely.

Notably, the interlayer distance (2.3 Å) measured by HRTEM between the Pt and Fe columns in Figure 3 is

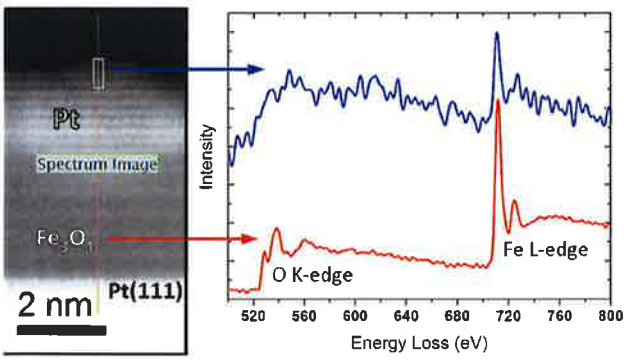

Figure 4. EELS spectra (after baseline subtraction) taken along the line scan as indicated in the energy range of the oxygen K-edge and Fe L-edge within the oxide film (red) and in the region of the surface of the Pt particle (blue).

considerably larger than 2 Å measured between those at the $Pt(111)/Fe_3O_4(111)$ interface (Figure 2), and 1.3 Å previously obtained for a FeO(111) monolayer film on Pt(111),[15] both structures having the Pt–Fe bonds. Our recent studies have shown that the FeO(111) monolayer readily transforms into the O-Fe-O trilayer structure at oxygen pressures above 10^{-2} mbar.[8a] Accordingly, the distance between the Fe and Pt layers increases from 1.3 Å to approximately 2.2 Å. Although the investigated sample has been passivated in UHV with a relatively thick amorphous carbon film, it appears that the original FeO film encapsulating Pt particles transforms here into the O-Fe-O trilayer upon adventitious reaction with air during the sample preparation (Supporting Information). The observed interlayer distance (2.3 Å) agrees well with the O-Fe-O-Pt(111) structure of the encapsulated film shown in Figure 3.

Finally, we address the source of the iron oxide encapsulating the Pt particles. Clearly, the amount of iron in the topmost layer in the pristine film (that is, $^1/_4$ ML), which is laterally contracted upon Pt deposition and annealing (see the above discussion), is not sufficient to cover a whole particle with a Fe monolayer. Therefore, there must be another source of iron ultimately encapsulating the Pt particle upon high-temperature annealing. Two scenarios could be envisioned: either Fe from the layer(s) underneath the particle migrates through the particle (virtually via alloying), or Fe migrates onto the Pt surface from the surrounding area. Previously, on the basis of high-energy electron diffraction measurements of $Pd/TiO_2(110)$, it has been proposed that the encapsulating material is transported by surface migration.[16] It should be mentioned, however, that TiO_2 single crystals normally possess extra Ti atoms located in interstitial sites in the bulk that readily migrate towards the surface upon heating.[17] In contrast, the thin $Fe_3O_4(111)$ films, prepared under well-controlled conditions, are essentially stoichiometric.

Thorough inspection of numerous STEM images revealed substantial contrast variations in the regions surrounding Pt particles (Figure 5). The annular bright field (ABF) and HAADF STEM images indicated a loss of iron atoms and lack of ordering in those areas (a similar picture was also observed underneath the particles, but we assign this effect to the uncovered oxide areas in front and/or behind the imaged Pt particle, as the images are recorded in projection). These findings favor the conclusion that the encapsulation proceeds through surface migration of Fe species from the oxide onto the Pt particle surface.

In summary, we show that a symbiosis of advanced methods of scanning probe and electron microscopies and well-defined model systems provides a detailed picture of interfaces in nanostructured catalytic systems. This was demonstrated for Pt nanoparticles supported on a well-ordered iron oxide thin film that undergo encapsulation by supporting oxide in the course of strong metal–support interactions. Furthermore, it is possible to reconstruct the localization of the oxide support material flowing over the metal particle. It appears that charge transfer from a transition metal oxide to highly electronegative Pt maximizes the number of platinum–cation (in this case, Fe) contacts at the interface. Depending on the chemical potential of reacting

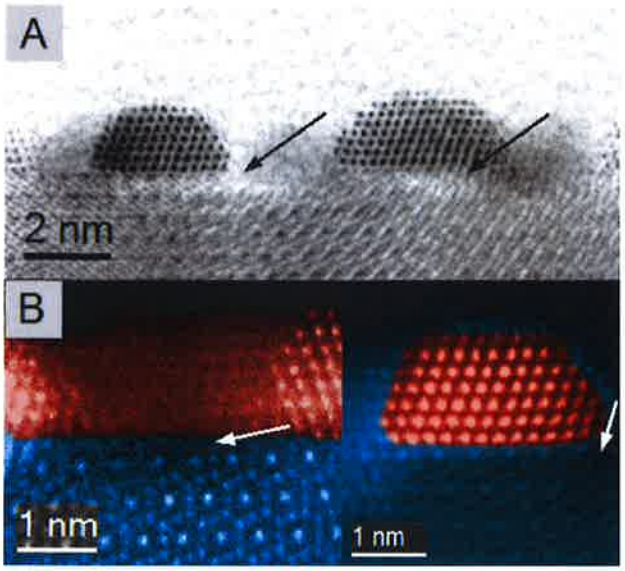

Figure 5. A) ABF and B) colorized HAADF STEM images. Arrows indicate a lower contrast and a decrease of ordering in the Fe_2O_3 film in the region of the Pt particle.

gases, phase separation into thicker layers of oxide and bare metal particles may become more favorable. The results provide additional information for theory to construct a detailed energetic picture of formation, stability, and effect of complex interfaces in catalysis.

Received: January 10, 2014
Revised: March 25, 2014
Published online: May 19, 2014

Keywords: heterogeneous catalysis · high-resolution electron microscopy · metal–support interactions · model systems · ultrathin oxide films

[1] S. J. Tauster, *Acc. Chem. Res.* **1987**, *20*, 389–394.
[2] a) F. Solymosi, *Catal. Rev.* **1968**, *1*, 233–255; b) G. L. Haller, D. E. Resasco in *Advances in Catalysis, Vol. 36* (Eds.: H. P. D. D. Eley, B. W. Paul), Academic Press, New York, **1989**, pp. 173–235; c) A. A. Slinkin, E. A. Fedorovskaya, *Russ. Chem. Rev.* **1971**, *40*, 860; d) G.-M. Schwab in *Advances in Catalysis, Vol. 27* (Eds.: H. P. D. D. Eley, B. W. Paul), Academic Press, New York, **1979**, pp. 1–22; e) F. F. Vol'kenshtein, *Russ. Chem. Rev.* **1966**, *35*, 537; f) H.-J. Freund, G. Pacchioni, *Chem. Soc. Rev.* **2008**, *37*, 2224–2242; g) Q. Fu, T. Wagner, *Surf. Sci. Rep.* **2007**, *62*, 431–498.
[3] a) E. J. Braunschweig, A. D. Logan, A. K. Datye, D. J. Smith, *J. Catal.* **1989**, *118*, 227–237; b) M. Behrens, F. Studt, I. Kasatkin, S. Kühl, M. Hävecker, F. Abild-Pedersen, S. Zander, F. Girgsdies, P. Kurr, B.-L. Kniep, M. Tovar, R. W. Fischer, J. K. Nørskov, R. Schlögl, *Science* **2012**, *336*, 893–897; c) S. Bernal, J. J. Calving, G. A. Cifredo, J. M. Rodríguez-Izquierdo, V. Perrichon, A. Laachir, *J. Catal.* **1992**, *137*, 1–11; d) M. Lewandowski, Y. N. Sun, Z. H. Qin, S. Shaikhutdinov, H. J. Freund, *Appl. Catal. A* **2011**, *391*, 407–410.
[4] M. Haider, H. Rose, S. Uhlemann, B. Kabius, K. Urban, *J. Electron Microsc.* **1998**, *47*, 395–405.
[5] a) J. Liu, *ChemCatChem* **2011**, *3*, 934–948; b) J. M. Thomas, C. Ducati, R. Leary, P. A. Midgley, *ChemCatChem* **2013**, *5*, 2560–2579; c) W. Zhou, I. E. Wachs, C. J. Kiely, *Curr. Opin. Solid State Mater. Sci.* **2012**, *16*, 10–22.
[6] a) O. Dulub, W. Hebenstreit, U. Diebold, *Phys. Rev. Lett.* **2000**, *84*, 3646–3649; b) Z. H. Qin, M. Lewandowski, Y. N. Sun, S. Shaikhutdinov, H. J. Freund, *J. Phys. Chem. C* **2008**, *112*, 10209–10213.
[7] Z. H. Qin, M. Lewandowski, Y. N. Sun, S. Shaikhutdinov, H. J. Freund, *J. Phys. Condens. Matter* **2009**, *21*, 134019.
[8] a) Y.-N. Sun, L. Giordano, J. Goniakowski, M. Lewandowski, Z.-H. Qin, C. Noguera, S. Shaikhutdinov, G. Pacchioni, H.-J. Freund, *Angew. Chem.* **2010**, *122*, 4520–4523; *Angew. Chem. Int. Ed.* **2010**, *49*, 4418–4421; b) Y. N. Sun, Z. H. Qin, M. Lewandowski, E. Carrasco, M. Sterrer, S. Shaikhutdinov, H. J. Freund, *J. Catal.* **2009**, *266*, 359–368.
[9] M. Ritter, W. Weiss, *Surf. Sci.* **1999**, *432*, 81–94.
[10] V. V. Roddatis, D. S. Su, C. Kuhrs, W. Ranke, R. Schlögl, *Thin Solid Films* **2001**, *396*, 78–83.
[11] A. Sala, H. Marchetto, Z. H. Qin, S. Shaikhutdinov, T. Schmidt, H. J. Freund, *Phys. Rev. B* **2012**, *86*, 155430.
[12] a) J. Goniakowski, C. Noguera, *Phys. Rev. B* **2009**, *79*, 155433; b) J. Goniakowski, C. Noguera, L. Giordano, G. Pacchioni, *Phys. Rev. B* **2009**, *80*, 125403.
[13] S. Shaikhutdinov, M. Ritter, W. Weiss, *Phys. Rev. B* **2000**, *62*, 7535–7541.
[14] D. A. Muller, L. F. Kourkoutis, M. Murfitt, J. H. Song, H. Y. Hwang, J. Silcox, N. Dellby, O. L. Krivanek, *Science* **2008**, *319*, 1073–1076.
[15] Y. J. Kim, C. Westphal, R. X. Ynzunza, H. C. Galloway, M. Salmeron, M. A. Van Hove, C. S. Fadley, *Phys. Rev. B* **1997**, *55*, R13448–R13451.
[16] T. Suzuki, R. Souda, *Surf. Sci.* **2000**, *448*, 33–39.
[17] M. Bowker, P. Stone, P. Morrall, R. Smith, R. Bennett, N. Perkins, R. Kvon, C. Pang, E. Fourre, M. Hall, *J. Catal.* **2005**, *234*, 172–181.